UAV-Aided Localization and Communication: Joint Frame Structure, Beamwidth, and Power Allocation

Tianhao Liang, *Graduate Student Member, IEEE*, Tingting Zhang, *Member, IEEE*, Sheng Zhou, *Senior Member, IEEE*, Wentao Liu, Dong Li, *Senior Member, IEEE*, and Qinyu Zhang, *Senior Member, IEEE*

***Abstract*—In wireless sensors networks, integrating localization and communication technique is crucial for efficient spectrum and hardware utilizations. In this article, we present a novel framework of the unmanned aerial vehicle (UAV)-aided localization and communication for ground node (GN), where the average spectral efficiency (SE) is used to reveal the intricate relationship among the frame structure, channel estimation error, and localization accuracy. In particular, we first derive the lower bounds for channel estimation error and the 3-D location prediction error, respectively. Leveraging these comprehensive analysis, we formulate a problem to maximize the average SE in the UAV–GN communication, where the frame structure, beamwidth, and power allocation can be jointly optimized. Subsequently, we propose an efficient iterative algorithm to address this nonconvex problem with closed-form expressions for beamwidth design and power allocation. Numerical results demonstrate that the performance of our proposed method can approach the upper bound with low complexity, and achieve over 70% performance gain compared with communication-only benchmarks. In addition, the analysis highlights the dominated impacts of the Doppler effect on the average SE.**

***Index Terms*—Channel estimation, integrated localization and communication, spectral efficiency (SE), wireless sensor networks.**

Manuscript received 31 March 2024; revised 8 July 2024; accepted 26 July 2024. Date of publication 6 August 2024; date of current version 12 September 2024. This work was supported in part by the Major Key Project of PCL under Grant PCL2024A01, in part by the Natural Science Foundation of China under Grant 62171160 and Grant 62027802, in part by the Fundamental Research Funds for the Central Universities under Grant HIT. OCEF. 2022055, and in part by the Shenzhen Science and Technology Program under Grant KJZD20231023093055002, Grant KJZD20230923114804009, Grant ZDSYS20210623091808025, and Grant 2024KSYS023. The work of Sheng Zhou was supported by the Natural Science Foundation of China under Grant 62341108. The work of Wentao Liu and Dong Li was supported by the Science and Technology Development Fund, Macau, SAR, under Grant 0188/2023/RIA3. Recommended by Lead Guest Editor Fan Liu and Guest Editor Yuanhao Cui. *(Corresponding author: Tingting Zhang.)*

Tianhao Liang is with the School of Electronics and Information Engineering, Harbin Institute of Technology (Shenzhen), Shenzhen 518055, China, and also with the Guangdong Provincial Key Laboratory of Space-Aerial Networking and Intelligent Sensing, 518055, China (e-mail: liangth@stu.hit.edu.cn).

Tingting Zhang and Qinyu Zhang are with the School of Electronics and Information Engineering, Harbin Institute of Technology (Shenzhen), Shenzhen 518055, China, and also with the Pengcheng Laboratory, Shenzhen 150001, China (e-mail: zhangtt@hit.edu.cn; zqy@hit.edu.cn).

Sheng Zhou is with the Department of Electronic Engineering, Tsinghua University, Beijing 100084, China (e-mail: sheng.zhou@tsinghua.edu.cn).

Wentao Liu and Dong Li are with the School of Computer Science and Engineering, Macau University of Science and Technology, Macau 999078, China (e-mail: 2202853eii30001@student.must.edu.mo; dli@must.edu.mo).

Digital Object Identifier 10.1109/JSAS.2024.3439272

I. Introduction

A. Background and Motivation

ACCURATE localization and reliable communication are two fundamental aspects of mobile wireless sensor networks [2]. Localization typically involves determining the spatial coordinates of mobile sensors, while communication facilitates the exchange of information between sensor nodes, enabling data transmission, remote control, and collaboration [3]. However, the current design in sensor networks often treats localization and communication as separate entities, which results in high hardware costs and low spectral efficiency (SE).

Prompted by advanced technologies of the millimeter-wave (mmWave) and massive multiple-input multiple-output (MIMO) in the upcoming 6G, integrated localization and communication systems are promising in many spectrum and cost-limited scenarios. However, obstacles on the ground may prevent the establishment of line-of-sight (LoS) links, leading to severe attenuation of mmWave signals and poor performance in localization and communication. Consequently, in applications with limited infrastructures, such as deep canyon environment monitoring, disaster life detection, and border target tracking, unpredictable difficulties may arise in supporting localization and communication [4].

Multiple fascinating advantages of unmanned aerial vehicles (UAVs), including high mobility, low cost, and fast deployment, have attracted substantial attention from both academia and industry [5]. UAVs can provide higher reliable LoS connected links and flexible topologies, presenting a cost-effective alternative to traditional infrastructures. In addition, UAVs have been proven to be significantly important in supporting localization and communication for ground devices out of the coverage of terrestrial networks [6] [7].

The bistatic channel estimation for communication in multi-antenna systems can be regarded as an integrated localization and communication process, where localization parameters, such as distance, time of arrival [8], and angle of arrival [9], can be obtained simultaneously from the channel state information (CSI). As UAVs can offer high-quality connections connected, they are also highly attractive for the integrated sensing, localization and communication technologies [10], [11]. Nevertheless, the high mobility inevitably contributes to nonnegligible Doppler effects, indicating a strongly time-variant characteristic of the channel. To mitigate this and achieve low channel estimation error, increasing the pilot overhead of the time frame is effective, which however will reduce the SE. Therefore, investigating the frame structure design, channel estimation, and wireless resource allocation in UAV-aided localization and communication system to achieve a high system SE is a particularly challenging task.

B. Related Work

Many efforts have been dedicated to optimizing the time frame structure for accurate channel estimation and data transmission. Mirhosseini et al. [12] investigated the channel estimation accuracy with respect to the pilot length and base stations density. Kang et al. [13] optimized the channel estimation time to improve data rates, where the duration of channel estimation was determined by comparing the predicted and the current data rate. Furthermore, they extended this investigation to the multiuser scenario in [14]. However, these investigations were limited to static communications. For dynamic scenarios, Mousaei and Smida [15] investigated frame structures to improve the achievable rate in both block and continuous fading, revealing the relationship of channel estimation error and frame structure. Building on this study, Cao et al. [16] proposed a time frame structure optimization problem to maximize the system throughput while guaranteeing the latency, and provided two frame structures for different scenarios. However, these studies focused exclusively on simple single-antenna systems. To address this limitation, Choi and Park [17] enhanced the sum SE and maximum error probability in the MIMO system by establishing a function between channel coefficients, precoders, error probabilities, and achievable SE. Nevertheless, this study assumed the prefect CSI. In addition, despite the frame structure and resource allocation strategies designed in the above studies from different perspectives, localization operations are rarely discussed, and 3-D scenarios are not investigated.

Based on the fact that the antenna phased shifts can be expressed as a function of receiver location [18], Li et al. [19] proposed a position-aided channel estimation method for high-speed railways, where the antenna array was divided into two parts for localization and communication, respectively. They also derived the relationship of mobility and throughput. However, this work required large-scale antennas arrays, making it unsuitable for the low-cost wireless sensor networks. Kwon et al. [20] optimized the pilot overhead by the cooperative beamforming and power allocation. However, this framework was designed for scenarios with sufficient infrastructures. In addition, Zhu et al. [21] utilized a full-duplex UAV as the aerial relay to increase the communication capacity under a 3-D channel model. The UAV location was optimized together with the CSI-based beamforming and power control. However, the UAV was assumed to be fixed in the air. In practice, the impacts of mobility in the UAV-involved network cannot be ignored. In such scenarios, CSI-based beamforming becomes computationally intensive and inaccurate due to the rapidly evolving channel conditions. To handle the channel uncertainty, it will incur a substantial overhead on channel estimation and localization. Location-aware beamforming can be adopted to reduce the beam swapping time and enhance the accuracy of beam alignment. Maschietti et al. [22] investigated a location-aided beam alignment for fast link establishment and provided a robust scheme by Bayesian team decision, but they only considered the static scenario. Mohammadi et al. [23] proposed a location-aware beamforming method for UAV communications by utilizing a spatial estimation method. However, they also assumed perfect CSI.

C. Main Contributions

Generally, for maximizing the SE, most investigations primarily focus on communication perspectives, while the localization is rarely researched. Moreover, the Doppler effect and CSI estimation error, which have huge impacts on the performance of localization and communication, are often ignored in dynamic networks. In this article, we investigate both channel and localization estimation in a UAV-involved network, and analyze the impacts of the Doppler effects for the system SE. To the best of the authors' knowledge, this article is one of the first comprehensive studies on the joint frame structure, beamforming, and power optimization to maximize SE in such system. In particular, we aim to reveal the relationship among channel estimation, localization, and communication in UAV-aided localization and communication systems. The main contributions of this article are summarized as follows.

1) We first elaborate on the settings and process of the UAV-aided localization and communication framework. Then, we derive the error bounds for channel estimation and 3-D location accuracy in terms of signal-to-noise ratio (SNR) and time frame structure. The relationship between localization and communication can be drawn leveraging those bounds. Subsequently, we formulate a joint frame structure, beamforming, and power optimization problem to maximize the average SE.
2) Building on the comprehensive analysis presented, we propose an efficient iterative method to solve the proposed optimization problem. This method employs relaxation and approximation strategies for determining transmission and pilot duration. Remarkably, the beamwidth and power allocation are expressed by closed forms to ensure practical feasibility and computational efficiency.
3) Finally, we conduct extensive simulations to demonstrate the advantages of our proposed approach compared to four benchmarks. The results showcase that the performance of integrated localization and communication

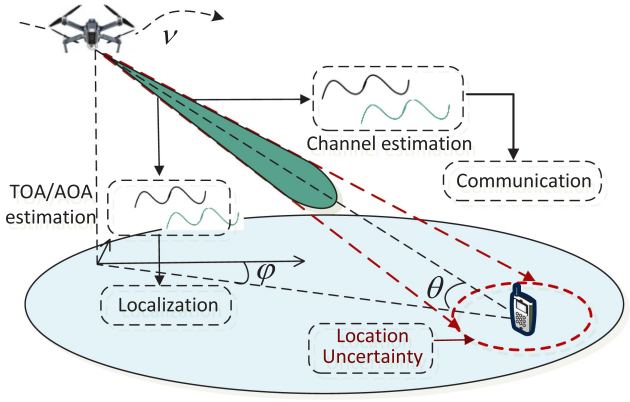

Fig. 1. UAV-aided localization and communication in dynamic scenario.

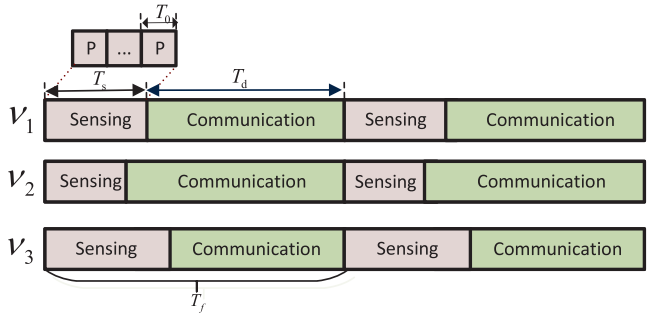

Fig. 2. Illustrated time frame structure with different relative velocities of UAV-to-GN downlink communication, where the relative velocity is calculated by $\boldsymbol{\nu}_{\mathrm{u}} - \boldsymbol{\nu}_{\mathrm{n}}$.

approach is close to the upper bound and significantly outperforms communication-only strategy, with gains exceeding 70% in average SE.

The rest of this article is organized as follows. Section II introduces the detailed system model and formulates the problem of the UAV-aided localization and communication network. Section III presents an efficient iterative algorithm to solve this optimization problem. Section IV demonstrates the simulation results. Finally, Section V concludes this article.

Notations: We use lowercase and uppercase bold symbols, and calligraphic uppercase characters to denote vectors, matrices, and sets, respectively. The term $(\cdot)^{\mathrm{T}}$ and $\|\cdot\|$ denote the transpose and Euclidean norm of its argument, respectively. The notation $\mathbb{E}(\cdot)$, $\mathrm{tr}(\cdot)$, and $\lfloor\cdot\rfloor$ are the expectation operator, the trace of a square matrix, and floor function, respectively.

II. System Model

We consider a point-to-point UAV-aided localization and communication process, as depicted in Fig. 1. This involves a UAV equipped with uniform planar array (UPA) employing $N_{\mathrm{t}} = M \times N$ antennas to assist the localization and communication of the ground node (GN), which is equipped with a single antenna with omnidirectional unity gain. We assume that the beamwidth of the UPA is adjustable. Without loss of generality, we consider downlink communication in the 3-D Cartesian coordinate system, where the GN receives the signal from the UAV for localization and communication. Moreover, we assume that the overhead of CSI feedback from the GN to UAV can be ignored, and the channel between UAV and GN is LoS.

The location and velocity of the UAV at time t are denoted by $\mathbf{x}_{\mathrm{u}}(t) = [p_{\mathrm{u}}^x(t), p_{\mathrm{u}}^y(t), p_{\mathrm{u}}^z(t)]^{\mathrm{T}}$ and $\boldsymbol{\nu}_{\mathrm{u}}(t) = [\nu_{\mathrm{u}}^x(t), \nu_{\mathrm{u}}^y(t), \nu_{\mathrm{u}}^z(t)]^{\mathrm{T}}$, respectively. Similarly, let $\mathbf{x}_{\mathrm{n}}(t) = [p_{\mathrm{n}}^x(t), p_{\mathrm{n}}^y(t), p_{\mathrm{n}}^z(t)]^{\mathrm{T}}$ and $\boldsymbol{\nu}_{\mathrm{n}}(t) = [\nu_{\mathrm{n}}^x(t), \nu_{\mathrm{n}}^y(t), \nu_{\mathrm{n}}^z(t)]^{\mathrm{T}}$ denote the location and velocity of the GN, respectively.

A. Communication Model

In the considered system, the UAV transmits signal $\mathbf{s}(t) = \mathbf{w}(t)s(t)$ to the GN with power $P(t)$, where $\mathbf{w}(t) \in \mathbb{C}^{N_{\mathrm{t}}\times 1}$ is the transmitted beamforming vector, and $\mathbb{E}(|\mathbf{s}(t)|^2) = 1$. Thus, the received signal of this multiple-input single-output system during the tth time slot can be expressed by

$$r(t) = \sqrt{P(t)}\mathbf{h}(t)\mathbf{s}(t) + n(t) \tag{1}$$

where $\mathbf{h}(t) \in \mathbb{C}^{1\times N_{\mathrm{t}}}$ is the channel vector between the UAV and the GN, and $n(t)$ is the white Gaussian noise at the receiver having zero mean and power σ_0^2. The current channel vector can be expressed by

$$\mathbf{h}(t) = \sqrt{\beta(t)}h(t)\mathbf{a}_{\mathrm{t}}^{\mathrm{H}}(\theta(t), \varphi(t)) \tag{2}$$

where $\beta(t) = \beta_0/d(t)^2$ is the large-scale channel fading with the distance between UAV and GN $d(t) = \sqrt{(p_{\mathrm{u}}^x(t) - p_{\mathrm{n}}^x(t))^2 + (p_{\mathrm{u}}^y(t) - p_{\mathrm{n}}^y(t))^2 + (p_{\mathrm{u}}^z(t) - p_{\mathrm{n}}^z(t))^2}$. The term β_0 represents the channel power at the reference distance 1 m. $h(t)$ is the small-scale Rician fading channel gain,[1] and $\mathbf{a}_{\mathrm{t}}(\theta(t), \varphi(t)) \in \mathbb{C}^{N_{\mathrm{t}}\times 1}$ are the array steering vectors of azimuth angle of departure (AoD) φ and elevation AoD θ.

The simplified antenna gain model of this article can be expressed according to [24]:

$$G(\theta(t), \varphi(t)) = \begin{cases} \frac{G_0}{\Phi(t)^2}, & \varphi(t) - \Phi(t) < \varphi(t) < \varphi(t) + \Phi(t) \\ & \text{and } \theta(t) - \Phi(t) < \theta(t) < \theta(t) + \Phi(t) \\ 0, & \text{otherwise} \end{cases} \tag{3}$$

where $2\Phi(t) \in (0, \pi)$ is the same half-power beamwidth of the antenna on azimuth and elevation, and G_0 is a gain constant. The antenna in the GN is omnidirectional with unit gain. Then, the instantaneous SNR can be computed by

$$\gamma(t) = \frac{P(t)G_0\beta_0}{\Phi(t)^2 d(t)^2 \sigma_0^2}. \tag{4}$$

The time frame structure is illustrated in Fig. 2, where the GN takes T_{s} to estimate the CSI during the sensing phase, which comprises k orthogonal pilots with the minimum time slot T_0. The estimated CSI is transmitted to the UAV immediately via the backhaul link. Subsequently, the UAV executes channel and localization estimation, and then employs beamforming and power control to build up a communication link with the GN for data transmission. The term T_{d} represents the duration

[1]The channel fading between GN and each antenna element at the UAV is highly correlated. Therefore, we use $h(t)$ to describe the LoS channel.

of data transmission. The channel is assumed to be correlated within a frame, maintaining coherence over the duration T_f, which is influenced by the Doppler effect of the connection link. As illustrated, the time frame structure will vary according to different dynamic behaviors.

B. Channel Estimation

Due to the time-varying characteristics of the proposed scenario caused by the mobility of the UAV, the CSI will soon become outdated, resulting in the high estimation error. Typically, the channel estimation error is caused by two factors [25]. The first is the noise, and the second is the rapid temporal variation of channel, reflected in the Doppler effect. We denote $\mathbf{h}_{1:t} = [h(1), \ldots, h(t)]^{\mathrm{T}}$ as the true channel vector for time 1 to time t, and $\widehat{\mathbf{h}}_{1:t}$ as our estimated channel. Then, the channel estimation error can be expressed as

$$\Delta\mathbf{h}_{1:t} = \widehat{\mathbf{h}}_{1:t} - \mathbf{h}_{1:t} = \Delta\mathbf{h}^{\mathrm{n}}_{1:t} + \Delta\mathbf{h}^{\mathrm{D}}_{1:t} \tag{5}$$

where $\Delta\mathbf{h}^{\mathrm{n}}_{1:t}$ is the channel mismatch caused by noise, and $\Delta\mathbf{h}^{\mathrm{D}}_{1:t}$ is the error due to temporal variation.

Proposition 1: Given the pilot length T_{s} with k orthogonal symbols of time frame with duration T_f, the channel estimation minimum mean square error (MMSE) at the end of this frame, which corresponds to the $(k+n)$th symbol, can be expressed as

$$\delta^2_{\mathbf{h}} = \underbrace{\frac{1}{1+k\gamma}}_{\text{noise}} + \underbrace{\frac{2k\gamma\left(1-\alpha_{k,k+n}\right)}{1+k\gamma}}_{\text{Doppler}} \tag{6}$$

where $\alpha_{k,k+n}$ is the correlation function between the channel at symbol k and symbol $k+n$ with $\alpha_{k,k+n} = \kappa^{\frac{nf_d}{0.423B}}$, and γ is the SNR of this frame. The term $\kappa \in (0,1)$ is the level of correlation, and f_d and B are the Doppler frequency shift and system bandwidth, respectively.

Proof: See Appendix A. ■

C. Localization Estimation and Prediction

For localization, the received signal at the GN from antenna j of the UAV can be modeled as

$$r_j(t) = \sum_{l=1}^{L} a_j^{(l)} s(t - \tau_j^{(l)}) + n(t)$$

where l denotes the number of multipath components, and $s(t)$ is the known pilot signal. Parameters $a_j^{(l)}$ and $\tau_j^{(l)}$ are the amplitude and delay of the lth path, respectively. Note that the first path can be easily detected due to high-quality LoS channel. Consequently, the phase ϕ_j and propagation delay τ_j can be extracted from the measurement model. According to the geometry of the UPA and the relative position, the relationship between phase and relative angle can be expressed as

$$\phi_j(t) = \phi_0(t) - \frac{2\pi f_c d_j}{c}\cos\left(\varphi(t) - \vartheta_j\right)\cos(\theta(t))$$

where $\phi_0(t)$ is the reference phase. f_c and c are the carrier frequency and speed of light, respectively. The term d_j and ϑ_j are the distance and angle between reference point and antenna j, respectively.

The motion model of UAV and GN can be expressed as

$$\mathbf{x}_{\mathrm{m}}(t) = \mathbf{x}_{\mathrm{m}}(t-1) + \boldsymbol{\nu}_{\mathrm{m}}(t)T_0 + \boldsymbol{\omega}(t) \tag{7}$$

where $\mathrm{m} = \{\mathrm{u}, \mathrm{n}\}$ is the index of UAV or GN, and $\boldsymbol{\omega}(t) = [\omega_x(t), \omega_y(t), \omega_z(t)]^{\mathrm{T}}$ is the transition noise vector along the x-axis, y-axis, and z-axis direction, which are assumed to be independent Gaussian distribution with zero mean and variance σ_x^2, σ_y^2, and σ_z^2.

According to our settings, the estimation parameters for localization at time t include time delay $\tau(t)$, elevation angle $\theta(t)$, and azimuth angle $\varphi(t)$. Therefore, the localization parameter space can be defined as

$$\boldsymbol{\Theta}(t) = [\tau(t), \theta(t), \varphi(t)]^{\mathrm{T}}. \tag{8}$$

Let $\widehat{\mathbf{x}}_{\mathrm{m}}$ denote the estimated location of the UAV and GN. In this article, we use the localization MSE $L_e^2(t) = \mathbb{E}\{\|\mathbf{x}_{\mathrm{m}}(t) - \widehat{\mathbf{x}}_{\mathrm{m}}(t)\|^2\}$ to evaluate the localization performance, which is determined by the on-board inertial and signal measurements between the UAV and GN.

We derive the posterior Cramér–Rao bound (PCRB) as the lower bound of the estimator variance in dynamic scenarios, which has been proven to effectively reflect practical localization results for a large number of measurements [26], [27]. The equivalent Fisher information matrix (FIM) of $\boldsymbol{\Theta}(t)$ can be expressed as a block diagonal matrix by chain rules from time 1 to time t with[2]

$$\mathbf{J}_{\mathrm{m}} = \begin{bmatrix} \mathbf{J}_{1,1} & \mathbf{C}_{1,2} & 0 & \cdots & 0 \\ \mathbf{C}_{1,2}^{\mathrm{T}} & \mathbf{J}_{2,2} & \mathbf{C}_{2,3} & \cdots & 0 \\ \vdots & \ddots & \ddots & \ddots & \vdots \\ 0 & \cdots & \mathbf{C}_{t-2,t-1}^{\mathrm{T}} & \mathbf{J}_{t-1,t-1} & \mathbf{C}_{t-1,t} \\ 0 & \cdots & 0 & \mathbf{C}_{t-1,t}^{\mathrm{T}} & \mathbf{J}_{t,t} \end{bmatrix}. \tag{9}$$

The element of $\mathbf{J}_{i,i}, i \in [1,t]$ is calculated by the FIM $\mathbf{J}^{\mathrm{p}}_{i,i}$ of measurement pilot signals and information $\mathbf{J}^{\mathrm{I}}_{i,i}$ from the on-board inertial measurement unit. Then, we can obtain the expression as follows:

$$\mathbf{J}_{i,i} = \begin{cases} \mathbf{J}^{\mathrm{p}}_{i,i} + \mathbf{J}^{\mathrm{I}}_{i,i}, & i \le T_{\mathrm{s}} \\ \mathbf{J}^{\mathrm{I}}_{i,i}, & T_{\mathrm{s}} < i \end{cases} \tag{10}$$

where the 3-D measurement matric can be characterized by [9]

$$\mathbf{J}^{\mathrm{p}}_{i,i} = \lambda_i^r \mathbf{q}_{i,r}\mathbf{q}_{i,r}^{\mathrm{T}} + \lambda_i^\theta \mathbf{q}_{i,\theta}\mathbf{q}_{ij,\theta}^{\mathrm{T}} + \lambda_i^\varphi \mathbf{q}_{i,\varphi}\mathbf{q}_{i,\varphi}^{\mathrm{T}}. \tag{11}$$

The terms λ_i^r, λ_i^θ, and λ_i^φ are the ranging information of intensity and angle information from the signal, and $\mathbf{q}_{i,r}$, $\mathbf{q}_{i,\theta}$, and $\mathbf{q}_{i,r}$ are the related angular vectors. The ranging information can be obtained by $\lambda_{i,r} = \frac{8\pi^2\zeta^2(1-\chi^2)}{c^2}\gamma(i)$, $\lambda_{i,\theta} = \frac{8\pi^2(\zeta\chi+f_c)^2}{c^2}\gamma(i)\sum_{n=1}^{N_t} A_{n,i}$, and $\lambda_{i,\varphi} = \frac{8\pi^2(\zeta\chi+f_c)^2}{c^2}\gamma(i)\sum_{n=1}^{N_t} A_{n,i}$, where ζ, χ, are the related signal parameters, and $A_{n,i}$ is the parameter related with the geometry of antenna array [28].

[2]We assume that prediction is only related to adjacent time slots, indicating $\mathbf{C}_{i-k,i} = 0, k \ge 2$.

Proposition 2: The direction vectors of distance, elevation, and azimuth are given by

$$\mathbf{q}_{i,r} = \begin{bmatrix}\cos\theta(i)\cos\varphi(i) & \sin\theta(i)\cos\varphi(i) & \sin\varphi(i)\end{bmatrix}^{\mathrm{T}} \quad (12)$$

$$\mathbf{q}_{i,\theta} = \begin{bmatrix}-\frac{\cos\varphi(i)\sin\theta(i)}{d(i)} & -\frac{\sin\theta(i)\sin\varphi(i)}{d(i)} & \frac{\cos\theta(i)}{d(i)}\end{bmatrix}^{\mathrm{T}} \quad (13)$$

$$\mathbf{q}_{i,\varphi} = \begin{bmatrix}-\frac{\sin\varphi(i)}{d(i)\cos\theta(i)} & \frac{\cos\varphi(i)}{d(i)\cos\theta(i)} & 0\end{bmatrix}^{\mathrm{T}}. \quad (14)$$

Proof: See Appendix B. ■

The measurement noise from on-board sensor is also assumed to be independent Gaussian distribution with zero mean and variance σ_x^2, σ_y^2, and σ_z^2. Therefore, the second term in (10) can be expressed as $\mathbf{J}_{i,i}^{\mathrm{I}} = \mathrm{diag}\{\frac{1}{\sigma_x^2}, \frac{1}{\sigma_y^2}, \frac{1}{\sigma_z^2}\}$, and the cross information matrix $\mathbf{C}_{i-1,i}$ is expressed as

$$\mathbf{C}_{i-1,i} = -\mathrm{diag}\left\{\frac{1}{\sigma_x^2}, \frac{1}{\sigma_y^2}, \frac{1}{\sigma_z^2}\right\}. \quad (15)$$

According to the matrix chain and Schur complement rules, we can obtain the localization FIM at time t by

$$\mathbf{J}(\mathbf{x}_{\mathrm{m}}(t)) = \mathbf{J}_{t,t} - \mathbf{C}_{t-1,t}(\mathbf{J}(\mathbf{x}_{\mathrm{m}}(t-1)) + \mathbf{C}_{t-1,t-1})^{-1}\mathbf{C}_{t-1,t}^{\mathrm{T}} \quad (16)$$

in which $\mathbf{J}(\mathbf{x}_{\mathrm{m}}(1)) = \mathbf{J}_{1,1}$. Consequently, the localization error can be bounded by

$$L_e^2(t) \geq \mathrm{tr}\left\{\left[\mathbf{J}^{-1}(\mathbf{x}_{\mathrm{m}}(t))\right]\right\}. \quad (17)$$

D. Problem Formulation

To ensure robust performance, the worst localization accuracy for a frame with duration length T_f is considered in the beamwidth design. This leads to the beamwidth function denoted by $\Phi(L_e(T_f))$, which affects the antenna gain and results in a new SNR $\gamma(t)$ for the frame, given by

$$\gamma(t) = \frac{P(t)G_0\beta_0}{\Phi(L_e(T_f))^2 d(t)^2 \sigma_0^2}.$$

Therefore, the localization accuracy is determined by the time frame structure and current SNR. The obtained localization accuracy guides beamwidth design $\Phi(L_e(T_f))$, which leads to the changed antenna gain and new SNR.

In the following, we omit t for simplicity. Given the frame structure and resource allocation, the ergodic achievable SE can be expressed as [29]

$$\eta_{\mathrm{SE}} = \left(1 - \frac{T_{\mathrm{s}}}{T_f}\right)\log_2(1+\gamma_e) \quad (18)$$

where $\gamma_e = \frac{\gamma(1-\delta_{\mathbf{h}}^2)}{1+\gamma\delta_{\mathbf{h}}^2}$ is the effective SNR under current instantaneous SNR γ with channel estimation error $\delta_{\mathbf{h}}^2$.

Based on the abovementioned analysis, there exists a fundamental tradeoff between localization and communication, i.e., the higher pilot duration reduces data transmission time, leading to lower SE. However, it also contributes to higher localization accuracy and narrower beamwidth, which can increase SE from the SNR perspective. Therefore, careful design of frame structure, beamwidth, and power allocation has significant impacts on the localization accuracy and channel estimation error, which will reflect on the SE performance.

In this article, we aim to maximize the average SE, by optimizing the pilot and data transmission durations, transmitted antenna beamwidth, and transmitted power. Let $\mathbf{T}_{\mathrm{s}} = [T_{\mathrm{s}}(1), T_{\mathrm{s}}(2), \ldots, T_{\mathrm{s}}(N)]^{\mathrm{T}}$ and $\mathbf{T}_{\mathrm{d}} = [T_{\mathrm{d}}(1), T_{\mathrm{d}}(2), \ldots, T_{\mathrm{d}}(N)]^{\mathrm{T}}$ denote the variable vector of N frames of pilot length and transmission length, respectively. Denote $\mathbf{\Phi} = [\Phi(1), \Phi(2), \ldots, \Phi(N)]^{\mathrm{T}}$ and $\mathbf{P} = [P(1), P(2), \ldots, P(N)]^{\mathrm{T}}$ as the variable vector of beamwidth and power allocation, respectively. Then, this optimization problem can be formulated as

$$\max_{\mathbf{T}_{\mathrm{s}},\mathbf{T}_{\mathrm{d}},\mathbf{\Phi},\mathbf{P}} \quad \frac{1}{N}\sum_{i=1}^{N}\eta_{\mathrm{SE}}(i) \quad (19)$$

$$\text{s.t.} \quad \mathrm{C1}: \gamma_e(i) \geq \gamma_{\mathrm{th}} \quad \forall i \quad (19a)$$

$$\mathrm{C2}: T_{\mathrm{s}}(i) > 0, T_{\mathrm{d}}(i) > 0 \quad \forall i \quad (19b)$$

$$\mathrm{C3}: \frac{T_{\mathrm{s}}(i)}{T_0}, \frac{T_{\mathrm{d}}(i)}{T_0} \in \mathbb{Z} \quad \forall i \quad (19c)$$

$$\mathrm{C4}: \Phi_{\min} \leq \Phi(i) \quad \forall i \quad (19d)$$

$$\mathrm{C5}: P(i) > 0, \sum_{i=1}^{N} P(i) \leq P_{\max} \quad \forall i \quad (19e)$$

where C1 is the communication transmission constraint, C2 and C3 are constraints on pilot and transmission durations, and C4 shows that the constraint on beamwidth should be greater than the minimum beamwidth $\Phi_{\min}$, which is determined by the array size. The constraint C5 ensures that the transmitted powers are nonnegative and cannot exceed a maximum value, where $P_{\max}$ is the total transmitted powers of the UAV for N frames. Due to the nonconvex objective function and the presence of mixed discrete and continuous constraints, this optimization problem cannot be optimally solved using current optimization tools.

III. Iterative Algorithm

Given the interdependence of frame structure, beamwidth, and power allocation on SE, achieving a globally optimal solution is challenging. In this section, we propose an efficient iterative algorithm to obtain a suboptimal solution for problem (19). The algorithm sequentially maximizes SE by optimizing individual variables while keeping others fixed. Specifically, we first relax the constraints and approximate the objective function to optimize transmission duration. Subsequently, the pilot length is optimized by a specifical solver. Then, the closed-form expression of beamwidth is given using the geometric theory. Next, the optimal power allocation is provided using the Karush–Kuhn–Tucker (KKT) conditions. Finally, we analyze the complexity of overall algorithm.

A. Transmission Duration Determination

In this subsection, we determine the transmission duration with fixed other variables. Obviously, the system average SE is maximum when each frame i is maximized. Consequently, we

analyze the optimization method in one frame, and we omit the index i for simplicity.

Given the pilot length T_s, beamwidth Φ, and power allocation P, the γ is fixed and the SE of current frame is calculated by

$$\eta_{\mathrm{SE}} = \frac{T_\mathrm{d}}{T_\mathrm{s}+T_\mathrm{d}} \log_2\left(\frac{A_1}{A_2 - 2k\gamma^2\kappa^{T_\mathrm{d}A_3}}\right) \tag{20}$$

where $A_1 = 1+k\gamma+\gamma+k\gamma^2$, $A_2 = 1+k\gamma+\gamma+2k\gamma^2$, and $A_3 = \frac{f_d}{0.423BT_0}$.

To tackle the nonconvexity of (20), we employ the successive convex optimization method to approximate it with a convex form using the first-order Taylor expansion around a given local point T_d^r. Therefore, the approximated objective function can be expressed as

$$\tilde{\eta}_{\mathrm{SE}}^r = A_4^r\left(T_\mathrm{d} - T_\mathrm{d}^r\right) + A_5^r \tag{21}$$

where

$$A_4^r = -\frac{T_\mathrm{d}^r}{T_\mathrm{s}+T_\mathrm{d}^r}\log_2 e\left(\frac{2k\gamma^2\ln\kappa A_3\kappa^{T_\mathrm{d}^r A_3}}{A_2 - 2k\gamma^2\kappa^{T_\mathrm{d}^r A_3}}\right) \tag{22}$$

$$+\frac{T_\mathrm{s}}{T_\mathrm{s}+T_\mathrm{d}^r}\log_2\left(\frac{A_1}{A_2 - 2k\gamma^2\kappa^{T_\mathrm{d}^r A_3}}\right) \tag{23}$$

$$A_5^r = \frac{T_\mathrm{d}^r}{T_\mathrm{s}+T_\mathrm{d}^r}\log_2\left(\frac{A_1}{A_2 - 2k\gamma^2\kappa^{T_\mathrm{d}^r A_3}}\right). \tag{24}$$

Moreover, there exists a maximum transmission duration $T_\mathrm{d}^{\max}$, which is calculated by C1 as follows:

$$\gamma_{\mathrm{th}} \le \frac{\gamma\left(1-\delta_{\mathbf{h}}^2\right)}{1+\gamma\delta_{\mathbf{h}}^2}, \quad \delta_{\mathbf{h}}^2 \le \frac{\gamma-\gamma_{\mathrm{th}}}{\gamma+\gamma\gamma_{\mathrm{th}}}. \tag{25}$$

Plugging (6) into (25), we can obtain the maximum transmission duration by

$$T_\mathrm{d}^{\max} = \frac{\ln\left(\frac{2k\gamma+1}{1+k\gamma} - \frac{\gamma-\gamma_{\mathrm{th}}}{\gamma+\gamma\gamma_{\mathrm{th}}}\right)A_4}{\ln(\kappa)f_d} \tag{26}$$

where $A_4 = \frac{1+k\gamma}{2k\gamma}T_0$.

The constraint C3 renders the integer limitations of T_d^r. To address this, we relax this constraint into continuous space. Consequently, the optimization problem for one frame structure can be replaced by the following problem:

$$\max_{T_\mathrm{d}} \ \tilde{\eta}_{\mathrm{SE}}^r \quad \text{s.t.} \ \ 0 < T_\mathrm{d} \le T_\mathrm{d}^{\max}. \tag{27}$$

In this way, the optimization problem becomes a standard convex optimization problem, enabling us to solve it via CVX solver. Then, we can obtain the transmission duration $T_\mathrm{d}^* = T_0\lfloor\frac{T_\mathrm{d}}{T_0}\rfloor$.

B. Pilot Length Optimization

Similar to determining transmission duration, the system's average SE is maximized by ensuring that each frame's SE reaches its peak. Therefore, we will also optimize the pilot length in one frame while keeping other variables fixed. The average SE can be expressed as

$$\eta_{\mathrm{SE}} = \frac{n}{k+n}\log_2\left(\frac{k\gamma^2+k\gamma+B_1}{2k\gamma^2B_2+k\gamma+B_1}\right) \tag{28}$$

where n and k are the symbol numbers of transmission and pilot, respectively. The term $B_1 = \gamma+1$ and $B_2 = 1-\alpha_{n,k+n}$. Maximizing η_{SE} is equivalent to minimizing $-\eta_{\mathrm{SE}}$. Then, this subproblem can be reformulated as

$$\min_{T_\mathrm{s}} \ -\eta_{\mathrm{SE}} \quad \text{s.t.} \ \ T_\mathrm{s} > 0, \quad k = \frac{T_\mathrm{s}}{T_0}, k \in \mathbb{Z}. \tag{29}$$

Due to the complicated objective function (28), this is a standard nonlinear integer programming problem (NLIP), which is difficult to solve directly. In this article, we address this NLIP problem using NOMAD solver in MATLAB OPTI Toolbox, which can find solutions in several iterations. After that, we can obtain the optimal pilot length T_s^*.

C. Beamwidth Design

When the pilot and transmission duration are fixed, the channel estimation error decreases by increasing the SNR. According to our antenna model in (3), a narrower beamwidth corresponds to higher antenna gain. However, if the θ and φ are out of the beam, the antenna gain trends toward zero. That indicates that high localization accuracy offers the high beam alignment and small beamwidth, which contributes the high performance on the SNR of the connected link. Similar to the pervious descriptions, the average SE is maximized when the SE of each frame is maximized. Here, we provide a *proposition* to demonstrate the relationship between beamwidth and localization accuracy.

Proposition 3: Given data transmission duration T_d, pilot length T_s, and transmitted power P, we can obtain the localization accuracy of UAV and GN by (17), denoted by L_u^2 and L_n^2, respectively. Denote the horizontal distance between UAV and GN as $d_h = \sqrt{(p_\mathrm{u}^x(t)-p_\mathrm{n}^x(t))^2+(p_\mathrm{u}^y(t)-p_\mathrm{n}^y(t))^2}$. Then, the optimal beamwidth can be calculated in the following two cases.

1) *Case 1:* When $d_h \ge L_\mathrm{u}+2L_\mathrm{n}$

$$\Phi^* = \max\left\{\arctan\left(\frac{d_1}{d_z}\right) - \arctan\left(\frac{d_2}{d_z}\right), \Theta_{\min}\right\} \tag{30}$$

where $d_1 = d_h - L_\mathrm{u} + 2L_\mathrm{n}$, $d_2 = d_h - L_\mathrm{u} - 2L_\mathrm{n}$, and $d_z = p_\mathrm{u}^z - p_\mathrm{n}^z$.

2) *Case 2:* When $d_h \le L_\mathrm{u}+2L_\mathrm{n}$

$$\Phi^* = \max\left\{2\arctan\left(\frac{2L_\mathrm{n}}{p_\mathrm{u}^z - p_\mathrm{n}^z}\right), \Theta_{\min}\right\}. \tag{31}$$

Proof: The similar proof illustration can be found in Appendix B of our pervious investigation [7]. However, unlike the proof in our previous research, we consider the imperfection in UAV location in this article. Therefore, the optimal beamwidth should introduce the uncertainty of UAV location. ■

D. Power Allocation

Given other variables, a higher transmitted power will lead to a higher SNR, better localization accuracy, and a lower channel estimation error. Thus, the average SE monotonically increases with the transmitted power. Therefore, the maximum SE is achieved when the constraint C5 becomes an equality. To ensure the constraint C1, we can obtain the lower bound of transmitted power $P_{\min}(i)$ at each frame i by solving following equation:

$$D_1\gamma(i)^2+\gamma_{\text{th}}\left(k+1\right)\gamma(i)+\gamma_{\text{th}}=0 \tag{32}$$

where $D_1=2kB_2\gamma_{\text{th}}+2kB_2-k$. This equation can be easily proven to have one positive root. Then, this nonlinear convex subproblem can be formulated as an equivalent form

$$\begin{aligned}\min_{\mathbf{P}}.\quad & -\sum_{i=1}^{N}\eta_{\text{SE}}(i)\\ \text{s.t.}\quad & P_{\min}(i)-P(i)\le 0\quad \forall i\\ & \sum_{i=1}^{N}P(i)-P_{\max}=0\quad \forall i.\end{aligned} \tag{33}$$

Under this formulation, the power allocation of each frame can be determined using the Lagrangian multiplier method with KKT conditions. The Lagrangian function for this problem is expressed as

$$\begin{aligned}\mathcal{L}(\mathbf{P},\boldsymbol{\lambda},\mu)=&-\sum_{i=1}^{N}\eta_{\text{SE}}(i)+\sum_{i=1}^{N}\lambda(i)\left(P_{\min}(i)-P(i)\right)\\ &+\mu\left(\sum_{i=1}^{N}P(i)-P_{\max}\right)\end{aligned} \tag{34}$$

where $\lambda(i)\ge 0$ and μ are the Lagrangian multipliers. According to the KKT conditions, we have

$$\begin{cases}-\eta'_{\text{SE}}(i)-\lambda(i)+\mu=0\quad \forall i\\ \lambda(i)\left(P_{\min}(i)-P(i)\right)=0\quad \forall i\\ \sum_{i=1}^{N}P(i)-P_{\max}=0\end{cases} \tag{35}$$

where $\eta'_{\text{SE}}(i)=\frac{\partial\eta_{\text{SE}}(i)}{\partial P(i)}$ is the first derivative of $\eta_{\text{SE}}(i)$. To guarantee the solvability of this problem, the maximum power should satisfy $P_{\max}\ge\sum_{i=1}^{N}P_{\min}(i)$.

In the second equation of (35), if $P_{\max}\ge\sum_{i=1}^{N}P_{\min}(i)$, then $\lambda(i)=0$. By substituting $\lambda(i)$ into the first equation and combining it with the equations of the first condition in (35) and the third condition, we can solve for the $i+1$ variables with $i+1$ equations. Then, we can obtain the power allocation result of each frame with $P(i)^{\dagger}$. Consequently, the optimal power of each frame i is given by

$$P(i)^{*}=\max\left\{P(i)^{\dagger},P_{\min}(i)\right\}. \tag{36}$$

E. Overall Algorithm and Complexity Analysis

The overall iterative algorithm is summarized in Algorithm 1. Here, we present the analysis of the complexity for our proposed method. Denote I as the number of iterations for convergency.

TABLE I
MAIN SIMULATION PARAMETERS

Parameters	Value
Symbol period	$T_0=66.7$ (μs)
Carrier frequency	$f_c=4.9$ (GHz)
Effective bandwidth	$\zeta=1$ (MHz)
Antenna reference gain	$G_0=2.28$ [24]
Baseband carrier correlation	$\chi=\sqrt{0.32}$ [31]
Noise power	$\sigma_0^2=-110$ (dBm) [32]
channel gain at 1 m	$\beta_0=-80$ (dB)
Threshold of SNR	$\gamma_{\text{th}}=3$ (dB)
Number of antenna	$N_{\text{t}}=4\times 4$
Minimum beamwidth	$\Phi_{\min}=5^{\circ}$
Motion noise	$\sigma_x=\sigma_y=\sigma_z=0.005$ m
Channel correlation level	$\kappa=0.8$

Algorithm 1: Proposed efficient iterative algorithm.

1: Set the initial state$(\mathbf{T}_{\text{d}}^0,\mathbf{T}_{\text{s}}^0,\boldsymbol{\Phi}^0,\mathbf{P}^0)$ and the iteration number $I=1$.
2: **Repeat**
3: **for** $i=1:N$ **do**
4: Given $(\mathbf{T}_{\text{s}}^{I-1},\boldsymbol{\Phi}^{I-1},\mathbf{P}^{I-1})$, solve problem (27) for frame i to obtain the optimal transmission duration T_{d}^{*}, update $\mathbf{T}_{\text{d}}^{I}(i)=T_{\text{d}}^{*}$.
5: **end for**
6: **for** $i=1:N$ **do**
7: Given $(\mathbf{T}_{\text{d}}^{I},\boldsymbol{\Phi}^{I-1},\mathbf{P}^{I-1})$, solve problem (29) for frame i to obtain the optimal pilot length T_{s}^{*}, update $\mathbf{T}_{\text{s}}^{I}(i)=T_{\text{s}}^{*}$.
8: **end for**
9: **for** $i=1:N$ **do**
10: Given $(\mathbf{T}_{\text{d}}^{I},\mathbf{T}_{\text{s}}^{I},\mathbf{P}^{I-1})$, obtain the optimal beamwidth $\Phi^{*}(i)$ of frame i by (30) (31), update $\boldsymbol{\Phi}^{I}(i)=\Phi^{*}(i)$.
11: **end for**
12: Given $(\mathbf{T}_{\text{d}}^{I},\mathbf{T}_{\text{s}}^{I},\boldsymbol{\Phi}^{I})$, obtain the optimal power allocation result by (36), update into $\mathbf{P}^{I}$.
13: **Until** the objective function $\sum_{i=1}^{N}\eta_{\text{SE}}(i)$ converges.

For optimizing the transmission duration, the major complexity is solving N approximated convex problems with complexity $N\mathcal{O}(c(1))$, where $C(1)$ represents the computational complexity by employing interior-point method with one variable [30]. For optimizing the pilot length, the major complexity lies in solving the NLIP with complexity $N\mathcal{O}(\log_2 k(i))$, where $k(i)$ is the pilot length of frame i. The beamwidth and power allocation are determined by the closed form. Consequently, the total complexity of our proposed algorithm is $N\mathcal{O}(I(c(1)+\log_2 k(i)))$. This analysis highlights the low complexity of our proposed iterative method, which is essential for the real-time optimization of the computation limited devices in a high dynamic scenario.

IV. Numerical Simulations

In this section, we thoroughly evaluate the proposed UAV aided localization and communication method via numerical simulations. The size of the simulation scenario is $1000\text{m}\times 200\text{m}\times 100\text{m}$. Unless otherwise specified, the main simulation parameters are presented in Table I.

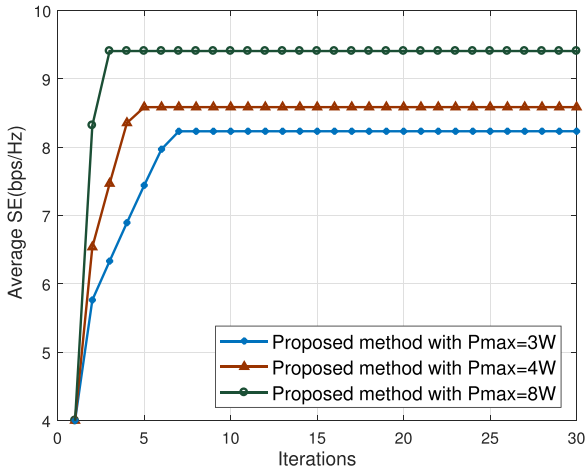

Fig. 3. Convergence performance of proposed method for various maximum total transmitted power.

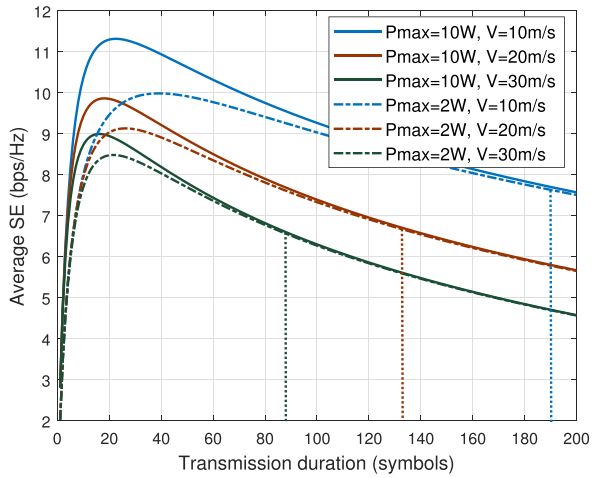

Fig. 4. Average SE performance of different conditions with fixed pilot length versus transmission duration.

To highlight the advantages of our framework, we compare the proposed efficient iterative method with a lower bound and three benchmark schemes in the following.

1) *Upper bound:* In this scheme, we employ an exhaustive method for this joint optimization problem, where the beamwidth and power allocation are executed using closed-form expressions in (30), (31), and (36).
2) *Benchmark 1:* In this scheme, we optimize the transmission duration, pilot length, and power allocation without considering the localization. This optimization problem is also solved using the similar iterative algorithm.
3) *Benchmark 2:* This scheme combines localization operation with a fixed frame structure. The beamwidth and power allocation are also given by our derivations.
4) *Benchmark 3:* In this scheme, we adopt the heuristic algorithm of particle swarm optimization (PSO) to find suboptimal solutions for the optimization method. The related parameters of this algorithm can be found in [33].

We first analyze the convergence behavior of our proposed iterative algorithm for various maximum transmitted power settings. This analysis is conducted with $N = 100$ and a UAV–GN relative velocity of 50 $\mathrm{m/s}$. As illustrated in Fig. 3, the average SE of GN always converges within ten iterations. Higher transmitted power levels, indicating the higher SNR, lead to faster convergence rates. Specifically, under the high SNR condition with $P_{\max} = 8$ W, our method converges within three iterations.

We also conducted a comparative evaluation of the computational time between the proposed method and PSO-based method with 200 particles. Using the same simulation platform, the proposed method only takes about 5 s, whereas the PSO-based method and the exhaustive research require over 50 and 300 s, respectively. This demonstrates the notable computational efficiency of our method.

Fig. 4 demonstrates the performance of the average SE with a fixed pilot length ($k = 5$) under different power limitations and relative velocities. As shown in this figure, higher power limitations lead to better performance, and there exists an optimal transmission duration T_{d}^* for each condition.

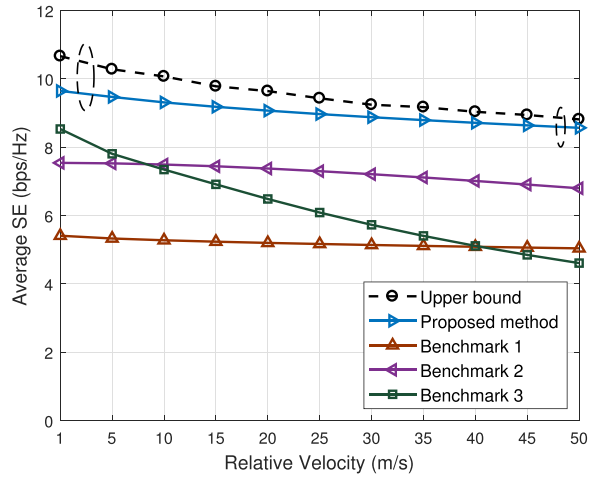

Fig. 5. Average SE performance of different methods versus UAV–GN relative velocities.

When $T_{\mathrm{d}} < T_{\mathrm{d}}^*$, the average SE increases with transmission duration due to the increase in the first term $(\frac{T_{\mathrm{s}}}{T_{\mathrm{s}}+T_{\mathrm{d}}})$ of (18). When $T_{\mathrm{d}} \geq T_{\mathrm{d}}^*$, the average SE decreases with transmission duration due to the worsened channel estimation and location prediction results. An interesting observation is that as the transmission duration increases, different power limitations converge in the same level. That can be explained by the effective SNR equation $\gamma_e = \frac{\gamma(1-\delta_{\mathbf{h}}^2)}{1+\gamma\delta_{\mathbf{h}}^2}$, which can be rewritten as $\gamma_e = \frac{(1-\delta_{\mathbf{h}}^2)}{\frac{1}{\gamma}+\delta_{\mathbf{h}}^2}$. Therefore, the effective SNR is highly dependent on the significant channel estimation error $\sigma_{\mathbf{h}}$. As observed in this figure (colored straight dotted-line), higher maximum power provides a greater range for convergence.

In Fig. 5, we evaluate the average SE performance across different UAV–GN relative velocities, comparing it against the upper bound and other benchmarks. Here, we set the maximum transmitted power $P_{\max} = 4$ W. The results demonstrate that our proposed method perform close to the upper bound, meaning that it is near-optimal, and achieves a remarkable over 75% performance gain compared with benchmark 1, highlighting the

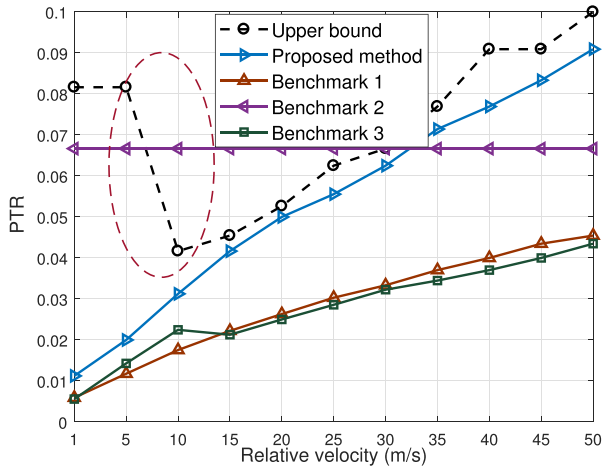

Fig. 6. PTR of different methods versus UAV–GN relative velocities.

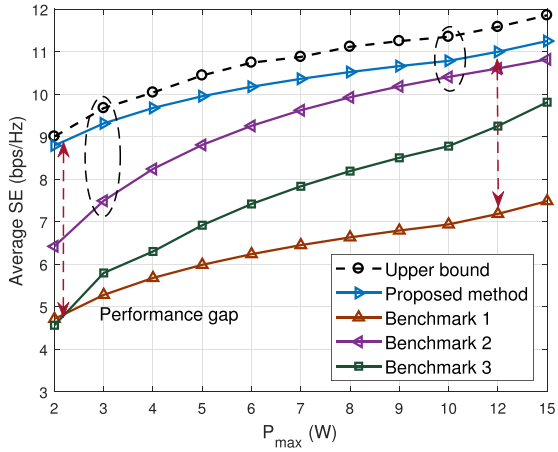

Fig. 7. Average SE performance of different methods versus maximum total transmitted powers.

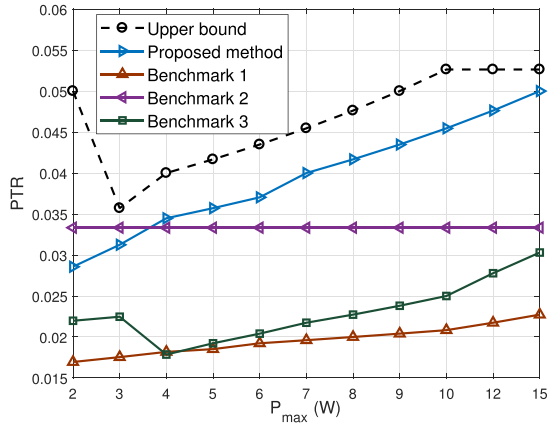

Fig. 8. PTR of different methods versus maximum total transmitted powers.

advantages of integrated localization and communication, which also aligns with the motivation of our investigation. Furthermore, our method shows significant performance gain compared to other benchmarks. As velocities increase, our results also display the greater robustness than benchmark 3, which fails to achieve reliable performance under lower effective SNR conditions.

Fig. 6 shows the pilot and transmission duration ratio (PTR) of different methods with the same conditions in Fig. 5. From the upper bound and our proposed method, we can find that our integrated localization and communication system increases the PTR compared with the communication-only method. This improvement is attributed to the fact that more pilot overhead can provide better localization accuracy, leading to a narrower beamwidth and higher SNR. There exists a change of the upper bound at the low-velocity region. The PTR decreases at relative velocity $10\ \mathrm{m/s}$. This is due to at this situation the SE is mainly influenced by the first term $\frac{T_\mathrm{s}}{T_\mathrm{s}+T_\mathrm{d}}$ of (18). That also verifies the performance gap in Fig. 5 between our method and the upper bound. As the velocity is increasing, the channel estimation error becomes grievous. The PTR should increase to improve the performance localization and channel estimation. The PTR of our method perform close to the upper bound at the high Doppler effect regions. In comparison to the fixed frame method, our proposed method can reduce the pilot overhead to guarantee high SE when the Doppler effect is small, while increasing the pilot ratio to compensate for the channel estimation mismatch when the Doppler effect is rigorous.

In Fig. 7, we evaluate the average SE of different methods with various transmitted power limitations. Here, we set the relative velocity at $10\ \mathrm{m/s}$, and the PTR of fixed frame is adjusted to $1/30$ in the benchmark 2. As expected, the average SE exhibits a positive correlation with the total transmitted power, and our proposed method consistently maintains a small gap with the upper bound. The benchmark 2 also demonstrates the good system performance, highlighting the importance of localization operation. As can be observed, the performance gap between our method and other benchmarks is smaller with the increasing SNR. That phenomenon showcases the effectiveness of our proposed method in low SNR regions.

In Fig. 8, we analyze the PTR for the simulation results in Fig. 7. Different from the result in Fig. 6, where increasing the pilot overhead mitigates the Doppler effect, this result reveals that it also needs to add the pilot ratio or reduce the duration of transmission as transmitted power increases. A shorter data transmission time implies reduced channel time-variant characteristics, indicating that the channel estimation interval has a significant impact compared to SNR in channel estimation. Note that there exists a decrease in the upper bound in this result. When the maximum total power $P_{\max} = 2\ \mathrm{W}$, the power allocated per time slot is very low, leading to poor channel estimation and localization accuracy. Under such condition, the upper bound seeks to reduce the transmission time to achieve better channel estimation error. Since the minimum pilot length is 1, the PTR rises with the decreased transmission duration. Conversely, when the $P_{\max} = 3\ \mathrm{W}$, improved channel estimation allows for longer data transmission duration, increasing the SE. In this scenario, the pilot length remains 1, resulting in the decreased PTR. As power limitations continue to increase, the PTR will increase to improve the effective SNR, eventually stabilizing at a fixed value when the channel conditions become optimal and further improvements are negligible ($P_{\max} \geq 10\ \mathrm{W}$).

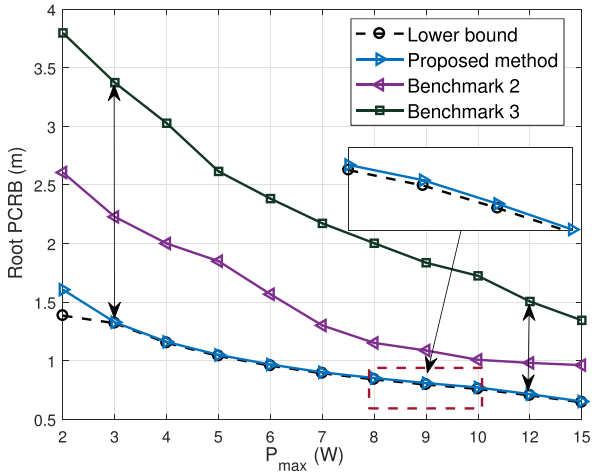

Fig. 9. Root PCRB of GN for different methods versus maximum total transmitted powers.

Finally, we show the root PCRB with different maximum total transmitted powers at the relative velocity of 10 m/s, to evaluate the localization performance of GN in Fig. 9. Obviously, the root PCRB decreases as the limited power increases due to the higher SNR. Our proposed method consistently approaches the optimal exhaustive search (lower bound) method and outperforms other benchmarks. At $P_{\max} = 2$ W, the lower bound achieves better performance than proposed method due to the high pilot duration, which also agrees the results in Fig. 8. In addition, the gap between proposed method and other benchmarks (indicated by the double arrow length) decreases with increasing the SNR conditions, highlighting the significance of the frame structure on localization performance in low SNR regions.

Based on above simulations, we can find that our joint time frame structure, beamwidth, and power optimization method can provide more flexible resource allocation form and significant performance improvement on SE. These comparisons also demonstrate the importance for localization by CSI, and showcase the integration gain of localization and communication. The proposed schemes can be also used as a guideline in the design of bistatic integrated sensing and communication systems [10].

V. Conclusion

In this article, we explored a UAV-aided localization and communication system. We formulated a joint frame structure, beamwidth, and power allocation optimization problem, to maximize the average SE of UAV–GN link. Given this nonconvex problem, we developed an efficient iterative algorithm to obtain suboptimal solutions. Base on the numerical results, we can draw following key conclusions.

1) The proposed method closely approaches the upper bound with remarkably low complexity, outperforming the communication-only method by over 70% in average SE.
2) The Doppler effect significantly influences channel estimation error, and the PTR should increase in both high dynamic and high SNR scenarios.
3) For a specifical scenario, there exists a unique frame structure to achieve optimal average SE.

These findings provide valuable insights for the design of bistatic integrated sensing and communication system. For potential future works, the multiuser, random signals, and trajectory management within integrated sensing, localization and communication scenario can be explored building on current framework.

Appendix A
Proof of Proposition 1

The channel estimation is executed by the receiving pilot symbols. Denote $\mathbf{x}_k = [x(1), x(2), \ldots, x(k)]^{\mathrm{T}}$ and $\mathbf{y}_k = [y(1), y(2), \ldots, y(k)]^{\mathrm{T}}$ as the input training and received symbol vectors, respectively. According to the MMSE rule [15], the estimated channel can be expressed as

$$\widehat{h}_k = \sqrt{\gamma}(1 + k\gamma)^{-1}\mathbf{x}_k^{\mathrm{H}}\mathbf{y}_k \tag{37}$$

where $(\cdot)^{\mathrm{H}}$ is the Hermitian operation. According to the received signal model in (1), $y(k) = \sqrt{\gamma}h(k)x(k) + n(k)$. In this article, we assume that $x(k)$ has unit mean square, which means $|\mathbf{x}_k|^2 = k$. Then, the estimated channel can be rewritten

$$\widehat{h}_k = \frac{k\gamma h(k)}{1 + k\gamma} + \frac{\sqrt{\gamma}\mathbf{x}_k^{\mathrm{H}}\mathbf{n}_k}{1 + k\gamma} \tag{38}$$

where $\mathbf{n}_k = [n(1), n(2), \ldots, n(k)]^{\mathrm{T}}$ is the noise vector.

In this article, the temporal channel correlation between two symbols can be modeled as a first-order Markov process [16]

$$h_n = \prod_{i=k+1}^{n} \alpha_{k,i} h_k + \sqrt{1 - \prod_{i=k+1}^{n} \alpha_{k,i}^2}\eta_i \tag{39}$$

where η_i is a Gaussian random variable with zero mean and unit variance, and $\alpha_{k,i} = \kappa^{\frac{f_d}{0.423B}}$ is the correlation factor between h_k and h_i. The term κ is the level of correlation, and f_d and B are the Doppler frequency shift and system bandwidth, respectively.

Therefore, given k pilot symbols, the channel estimation error at the symbol n can be calculated by

$$\begin{aligned}\delta_{\mathbf{h}} = h_n - \widehat{h}_k &= \prod_{i=k+1}^{n} \alpha_{k,i} h_k \\ &+ \sqrt{1 - \prod_{i=k+1}^{n} \alpha_{k,i}^2}\eta_i - \frac{k\gamma h(k)}{1 + k\gamma} + \frac{\sqrt{\gamma}\mathbf{x}_k\mathbf{n}_k}{1 + k\gamma}.\end{aligned} \tag{40}$$

We take the MSE of (40) to obtain $\mathbb{E}\{|\delta_{\mathbf{h}}|^2\}$ with

$$\begin{aligned}\delta_{\mathbf{h}}^2 &= \left(\prod_{i=k+1}^{n} \alpha_{k,i} - \frac{k\gamma}{1 + k\gamma}\right)\mathbb{E}\left\{|h_k|^2\right\} \\ &+ \left(1 - \prod_{i=k+1}^{n} \alpha_{k,i}^2 \mathbb{E}\left\{|\eta_n|^2\right\}\right) + \frac{k\gamma}{(1 + k\gamma)^2} \\ &= \frac{1}{1 + k\gamma} + \frac{2k\gamma\left(1 - \prod_{i=k+1}^{n} \alpha_{k,i}\right)}{(1 + k\gamma)} \\ &= \frac{1}{1 + k\gamma} + \frac{2k\gamma(1 - \alpha_{k,k+n})}{(1 + k\gamma)}.\end{aligned} \tag{41}$$

Thus, the proof of *Proposition 1* is completed.

APPENDIX B
PROOF OF PROPOSITION 2

We convert the parameter space $\boldsymbol{\Theta}(t)$ to the position coordinates, and show their relationships as follows:

$$c\tau(t) = \sqrt{\left(p_{\mathrm{u}}^{x}(t) - p_{\mathrm{n}}^{x}\right)^2 + \left(p_{\mathrm{u}}^{y}(t) - p_{\mathrm{n}}^{y}\right)^2 + \left(p_{\mathrm{u}}^{z}(t) - p_{\mathrm{n}}^{z}\right)^2} \tag{42}$$

$$\varphi(t) = \arctan\left(\frac{p_{\mathrm{u}}^{y}(t) - p_{\mathrm{n}}^{y}(t)}{p_{\mathrm{u}}^{x}(t) - p_{\mathrm{n}}^{x}(t)}\right) \tag{43}$$

$$\theta(t) = \arctan\left(\frac{p_{\mathrm{u}}^{z}(t) - p_{\mathrm{n}}^{z}(t)}{\sqrt{\left(p_{\mathrm{u}}^{x}(t) - p_{\mathrm{n}}^{x}\right)^2 + \left(p_{\mathrm{u}}^{y}(t) - p_{\mathrm{n}}^{y}\right)^2}}\right). \tag{44}$$

We omit t for simplicity. Without loss generality, we derive the direction vector for localization of GN as follows:

$$\mathbf{q}_r = \begin{bmatrix} \frac{\partial c\tau}{p_{\mathrm{n}}^{x}} \\ \frac{\partial c\tau}{p_{\mathrm{n}}^{y}} \\ \frac{\partial c\tau}{p_{\mathrm{n}}^{z}} \end{bmatrix} = \begin{bmatrix} -\frac{p_{\mathrm{u}}^{x} - p_{\mathrm{n}}^{x}}{d} \\ -\frac{p_{\mathrm{u}}^{y} - p_{\mathrm{n}}^{y}}{d} \\ -\frac{p_{\mathrm{u}}^{z} - p_{\mathrm{n}}^{z}}{d} \end{bmatrix} = \begin{bmatrix} -\cos\varphi\cos\theta \\ -\sin\varphi\cos\theta \\ -\sin\theta \end{bmatrix} \tag{45}$$

$$\mathbf{q}_\theta = \begin{bmatrix} \frac{\partial \theta}{p_{\mathrm{n}}^{x}} \\ \frac{\partial \theta}{p_{\mathrm{n}}^{y}} \\ \frac{\partial \theta}{p_{\mathrm{n}}^{z}} \end{bmatrix} = \begin{bmatrix} \frac{(p_{\mathrm{u}}^{x} - p_{\mathrm{n}}^{x})(p_{\mathrm{u}}^{z} - p_{\mathrm{n}}^{z})}{\sqrt{(p_{\mathrm{u}}^{x} - p_{\mathrm{n}}^{x})^2 + (p_{\mathrm{u}}^{y} - p_{\mathrm{n}}^{y})^2}\, d} \\ \frac{(p_{\mathrm{u}}^{y} - p_{\mathrm{n}}^{y})(p_{\mathrm{u}}^{z} - p_{\mathrm{n}}^{z})}{\sqrt{(p_{\mathrm{u}}^{x} - p_{\mathrm{n}}^{x})^2 + (p_{\mathrm{u}}^{y} - p_{\mathrm{n}}^{y})^2}\, d} \\ -\frac{(p_{\mathrm{u}}^{x} - p_{\mathrm{n}}^{x})^2 + (p_{\mathrm{u}}^{y} - p_{\mathrm{n}}^{y})^2}{d} \end{bmatrix} = \begin{bmatrix} \frac{\cos\varphi\sin\theta}{d} \\ \frac{\sin\varphi\sin\theta}{d} \\ -\frac{\cos\theta}{d} \end{bmatrix} \tag{46}$$

$$\mathbf{q}_\varphi = \begin{bmatrix} \frac{\partial \varphi}{p_{\mathrm{n}}^{x}} \\ \frac{\partial \varphi}{p_{\mathrm{n}}^{y}} \\ \frac{\partial \varphi}{p_{\mathrm{n}}^{z}} \end{bmatrix} = \begin{bmatrix} \frac{p_{\mathrm{u}}^{y} - p_{\mathrm{n}}^{y}}{\sqrt{(p_{\mathrm{u}}^{x} - p_{\mathrm{n}}^{x})^2 + (p_{\mathrm{u}}^{y} - p_{\mathrm{n}}^{y})^2}} \\ -\frac{p_{\mathrm{u}}^{x} - p_{\mathrm{n}}^{x}}{\sqrt{(p_{\mathrm{u}}^{x} - p_{\mathrm{n}}^{x})^2 + (p_{\mathrm{u}}^{y} - p_{\mathrm{n}}^{y})^2}} \\ 0 \end{bmatrix} = \begin{bmatrix} \frac{\sin\varphi}{d\cos\theta} \\ -\frac{\cos\varphi}{d\cos\theta} \\ 0 \end{bmatrix}. \tag{47}$$

Then, the proof of *Proposition 2* is completed.

REFERENCES

[1] T. Liang et al., "Joint frame structure and beamwidth optimization for integrated localization and communication," in *2024 IEEE Wireless Commun. Netw. Conf.*, 2024, pp. 1–6.

[2] J. Liu, P. Tong, X. Wang, B. Bai, and H. Dai, "UAV-aided data collection for information freshness in wireless sensor networks," *IEEE Trans. Wireless Commun.*, vol. 20, no. 4, pp. 2368–2382, Apr. 2021.

[3] F. Liu et al., "Integrated sensing and communications: Toward dual-functional wireless networks for 6G and beyond," *IEEE J. Sel. Areas Commun.*, vol. 40, no. 6, pp. 1728–1767, Jun. 2022.

[4] T. Liang, T. Zhang, and Q. Zhang, "Toward seamless localization and communication: A satellite-UAV NTN architecture," *IEEE Netw.*, vol. 38, no. 4, pp. 103–110, Jul. 2024.

[5] Q. Wu et al., "A comprehensive overview on 5G-and-beyond networks with UAVs: From communications to sensing and intelligence," *IEEE J. Sel. Areas Commun.*, vol. 39, no. 10, pp. 2912–2945, Oct. 2021.

[6] Y. Liu, Y. Wang, X. Shen, J. Wang, and Y. Shen, "UAV-aided relative localization of terminals," *IEEE Internet Things J.*, vol. 8, no. 16, pp. 12999–13013, Aug. 2021.

[7] T. Liang et al., "Age of information based scheduling for UAV aided localization and communication," *IEEE Trans. Wireless Commun.*, vol. 23, no. 5, pp. 4610–4626, May 2024.

[8] Y. Shen and M. Z. Win, "On the accuracy of localization systems using wideband antenna arrays," *IEEE Trans. Commun.*, vol. 58, no. 1, pp. 270–280, Jan. 2010.

[9] T. Liang, T. Zhang, J. Yang, D. Feng, and Q. Zhang, "UAV-aided positioning systems for ground devices: Fundamental limits and algorithms," *IEEE Internet Things J.*, vol. 9, no. 15, pp. 13470–13485, Aug. 2022.

[10] S. Lu et al., "Integrated sensing and communications: Recent advances and ten open challenges," *IEEE Internet Things J.*, vol. 11, no. 11, pp. 19094–19120, Jun. 2024.

[11] X. Jing, F. Liu, C. Masouros, and Y. Zeng, "ISAC from the sky: UAV trajectory design for joint communication and target localization," *IEEE Trans. Wireless Commun.*, early access, May 10, 2024, doi: 10.1109/TWC.2024.3396571.

[12] F. Mirhosseini, A. Tadaion, and S. M. Razavizadeh, "Spectral efficiency of dense multicell massive MIMO networks in spatially correlated channels," *IEEE Trans. Veh. Technol.*, vol. 70, no. 2, pp. 1307–1316, Feb. 2021.

[13] J. Kang, N. Garcia, H. Wymeersch, C. Fischione, G. Seco-Granados, and S. Kim, "Optimizing the mmWave channel estimation duration by rate prediction," *IEEE Commun. Lett.*, vol. 25, no. 2, pp. 555–559, Feb. 2021.

[14] J. Kang, H. Wymeersch, C. Fischione, G. Seco-Granados, and S. Kim, "Optimized switching between sensing and communication for mmWave MU-MISO systems," in *2022 IEEE Int. Conf. Commun. Workshops*, 2022, pp. 498–503.

[15] M. Mousaei and B. Smida, "Optimizing pilot overhead for ultra-reliable short-packet transmission," in *2017 IEEE Int. Conf. Commun.*, 2017, pp. 1–5.

[16] J. Cao et al., "Independent pilots versus shared pilots: Short frame structure optimization for heterogeneous-traffic URLLC networks," *IEEE Trans. Wireless Commun.*, vol. 21, no. 8, pp. 5755–5769, Aug. 2022.

[17] J. Choi and J. Park, "MIMO design for Internet of Things: Joint optimization of spectral efficiency and error probability in finite block-length regime," *IEEE Internet Things J.*, vol. 8, no. 20, pp. 15512–15521, Oct. 2021.

[18] B. Zhu, Z. Zhang, and J. Cheng, "Outage analysis and beamwidth optimization for positioning-assisted beamforming," *IEEE Commun. Lett.*, vol. 26, no. 7, pp. 1543–1547, Jul. 2022.

[19] T. Li, X. Wang, P. Fan, and T. Riihonen, "Position-aided large-scale MIMO channel estimation for high-speed railway communication systems," *IEEE Trans. Veh. Technol.*, vol. 66, no. 10, pp. 8964–8978, Oct. 2017.

[20] G. Kwon, A. Conti, H. Park, and M. Z. Win, "Joint communication and localization in millimeter wave networks," *IEEE J. Sel. Topics Signal Process.*, vol. 15, no. 6, pp. 1439–1454, Nov. 2021.

[21] L. Zhu, J. Zhang, Z. Xiao, X. Cao, X.-G. Xia, and R. Schober, "Millimeter-wave full-duplex UAV relay: Joint positioning, beamforming, and power control," *IEEE J. Sel. Areas Commun.*, vol. 38, no. 9, pp. 2057–2073, Sep. 2020.

[22] F. Maschietti, D. Gesbert, P. de Kerret, and H. Wymeersch, "Robust location-aided beam alignment in millimeter wave massive MIMO," in *2017 IEEE Glob. Commun. Conf.*, 2017, pp. 1–6.

[23] A. Mohammadi, M. Rahmati, and H. Malik, "Location-aware beamforming for MIMO-enabled UAV communications: An unknown input observer approach," *IEEE Sensors J.*, vol. 22, no. 8, pp. 8206–8215, Apr. 2022.

[24] Z. Yang et al., "Joint altitude, beamwidth, location, and bandwidth optimization for UAV-enabled communications," *IEEE Commun. Lett.*, vol. 22, no. 8, pp. 1716–1719, Aug. 2018.

[25] R. K. Mallik, M. R. Bhatnagar, and S. P. Dash, "Fractional pilot duration optimization for SIMO in Rayleigh fading with MPSK and imperfect CSI," *IEEE Trans. Commun.*, vol. 66, no. 4, pp. 1732–1744, Apr. 2018.

[26] T. Wang, H. Zhao, and Y. Shen, "High-accuracy localization using single-anchor ultra-wide bandwidth systems," in *2019 IEEE/CIC Int. Conf. Commun. China*, 2019, pp. 59–63.

[27] T. Wang, Y. Li, J. Liu, K. Hu, and Y. Shen, "Multipath-assisted single-anchor localization via deep variational learning," *IEEE Trans. Wireless Commun.*, vol. 23, no. 8, pp. 9113–9128, Aug. 2024.

[28] Y. Wang, Y. Wu, and Y. Shen, "On the resolution limits for MIMO localization," *IEEE Commun. Lett.*, vol. 23, no. 3, pp. 462–465, Mar. 2019.

[29] H. Ren, C. Pan, Y. Deng, M. Elkashlan, and A. Nallanathan, "Joint pilot and payload power allocation for massive-MIMO-enabled URLLC IIoT networks," *IEEE J. Sel. Areas Commun.*, vol. 38, no. 5, pp. 816–830, May 2020.

[30] S. Boyd and L. Vandenberghe, *Convex Optimization*. Cambridge, U.K.: Cambridge University Press, 2004.

[31] T. Zhang, A. F. Molisch, Y. Shen, Q. Zhang, H. Feng, and M. Z. Win, "Joint power and bandwidth allocation in wireless cooperative localization networks," *IEEE Trans. Wireless Commun.*, vol. 15, no. 10, pp. 6527–6540, Oct. 2016.

[32] D. Li, "Ergodic capacity of intelligent reflecting surface-assisted communication systems with phase errors," *IEEE Commun. Lett.*, vol. 24, no. 8, pp. 1646–1650, Aug. 2020.

[33] T. Liang, W. Liu, J. Yang, and T. Zhang, "Age of information based scheduling for UAV aided emergency communication networks," in *2022 IEEE Int. Conf. Commun.*, 2022, pp. 5128–5133.

Tianhao Liang (Graduate Student Member, IEEE) received the B.S. degree in electronic science and technology from Zhengzhou University, Zhengzhou, China, in 2019. He is currently working toward the Ph.D. degree in information and communication engineering with the School of Electronics and Information Engineering, Harbin Institute of Technology, Shenzhen, China.

From March 2023 to July 2023, he was a Visiting Student with the Department of Electronic Engineering and Beijing National Research Center for Information Science and Technology, Tsinghua University. His research interests include signal processing, UAV communication, integration of localization and communications, resource optimization, and UAV control.

Dr. Liang was the recipient of the Honorary Mention in the 2022 IEEE ComSoc Student Competition, as a Team Leader. He is currently a Reviewer and TPC Member of several conferences, such as Globecom, ICC, WCNC, VTC, ACC, and PIMRC.

Tingting Zhang (Member, IEEE) received the B.S. (with honors), M.S., and Ph.D. degrees in electronic engineering from the Harbin Institute of Technology (HIT), Harbin, China, in 2003, 2005, and 2009, respectively.

From 2009 to 2012, he was a Postdoctoral Research Fellow with the Communication Engineering Research Center, Shenzhen Graduate School, HIT. From 2012 to 2014, he was a Visiting Scholar with the Department of Electronic Engineering, University of Southern California, Los Angeles, CA, USA. He is currently a Professor with the Harbin Institute of Technology, Shenzhen, China. He is also a Professor with Peng Cheng Laboratory, Shenzhen. His research interests include wireless localization, integration of sensing and communication, and autonomous vehicle navigation and control.

Dr. Zhang is currently the Associate Editor of *Frontiers in Communications and Networks*, Guest Editor of *IEEE Communications Magazine* and *EURASIP Journal of Wireless Communications and Networks*, also Organizer and TPC Member for several international conferences, such as ICC, GLOBECOM, ICCC, and VTC. He was the recipient of the Outstanding Postdoctoral Award of HIT, Shenzhen Graduate School in 2011 and Shenzhen High-Level Talent Program award in 2012.

Sheng Zhou (Senior Member, IEEE) received the B.E. and Ph.D. degrees in electronic engineering from Tsinghua University, Beijing, China, in 2005 and 2011, respectively.

In 2010, he was a Visiting Student with the Wireless System Lab, Department of Electrical Engineering, Stanford University, Stanford, CA, USA. From 2014 to 2015, he was a Visiting Researcher with the Central Research Lab, Hitachi Ltd., Tokyo, Japan. He is currently an Associate Professor with the Department of Electronic Engineering, Tsinghua University. His research interests include cross-layer design for multiple antenna systems, mobile edge computing, vehicular networks, and green wireless communications.

Dr. Zhou was the recipient of the IEEE ComSoc Asia-Pacific Board Outstanding Young Researcher Award in 2017 and IEEE ComSoc Wireless Communications Technical Committee Outstanding Young Researcher Award in 2020.

Wentao Liu received the bachelor's degree in information engineering from Xi'an Jiaotong University, Xi'an, China, in 2016, and the master's degree in telecommunications from the Hong Kong University of Science and Technology, Hong Kong, China, in 2018. He is currently working toward the Ph.D. degree in electronic information technology with the Macau University of Science and Technology (MUST), Macau, China.

His research interests include UAV-assisted wireless network design and deep reinforcement learning.

Dong Li (Senior Member, IEEE) received the Ph.D. degree in electronics and communication engineering from Sun Yat-sen University, Guangzhou, China, in 2010.

Since 2010, he has been with the School of Computer Science and Engineering (formally, Faculty of Information Technology), Macau University of Science and Technology (MUST), Macau, China, where he is currently a Full Professor. In 2012, he held a Visiting Position with the Institute for Infocomm Research, Singapore. His current research interests include 6G wireless communications, battery-free Internet of Things (IoT), and wireless AI.

Dr. Li was the recipient of the MUST Best Research Output Award in 2022, the MUST Bank of China (BoC) Excellent Research Award in 2011, 2016, 2019, and 2021, the Best Paper Awards of IEEE ICCT 2023, IEEE HealthCom 2023, and MICCIS 2024, and the Distinguished Paper Award of IEEE GreenCom 2023. He has been listed among World's Top 2% Scientists recognized by Stanford University since 2020. He is currently an Editor for the IEEE MMTC Review, an Executive Board Member of the IEEE Macau Section, and a Member of the Association for Promotion of Science and Technology of Macau.

Qinyu Zhang (Senior Member, IEEE) received the bachelor's degree in communication engineering from the Harbin Institute of Technology (HIT), Harbin, China, in 1994, and the Ph.D. degree in biomedical and electrical engineering from the University of Tokushima, Tokushima, Japan, in 2003.

From 1999 to 2003, he was an Assistant Professor with the University of Tokushima. From 2003 to 2005, he was an Associated Professor with HIT Shenzhen Graduate School, and was the Founding Director with Communication Engineering Research Center, School of Electronic & Information Engineering (EIE). Since 2005, he has been a Full Professor, and is currently the Dean with EIE School. His research interests include aerospace communications and networks, wireless communications and networks, cognitive radios, signal processing and biomedical engineering.

Dr. Zhang is on the editorial board of some academic journals, such as *Journal on Communications*, *KSII Transactions on Internet and Information Systems*, Science China: *Information Sciences*, etc. He was the TPC Co-chair of IEEE/CIC ICCC'15, Symposium Co-chair of IEEE VTC'16 Spring, Associate Chair for Finance of ICMMT'12, Symposium Co-chair of CHINACOM'11, etc. He has been a TPC Member for INFOCOM, ICC, GLOBECOM, WCNC and other flagship conferences in communications. He was the Founding Chair of the IEEE Communications Society Shenzhen Chapter. He was the recipient of the National Science Fund for Distinguished Young Scholars, Young and Middle-aged Leading Scientist of China, the Chinese New Century Excellent Talents in University, etc., and obtained three scientific and technological awards from governments.